Published in final edited form as:
Nano Lett. 2010 July 14; 10(7): 2714–2720. doi:10.1021/nl1018468.

Immobilization and One-Dimensional Arrangement of Virus Capsids With Nanoscale Precision Using DNA Origami

Nicholas Stephanopoulos[1,‡], **Minghui Liu**[2,‡], **Gary J. Tong**[1], **Zhe Li**[2], **Yan Liu**[2], **Hao Yan**[2,*], and **Matthew B. Francis**[1,*]

[1]Department of Chemistry, University of California, Berkeley, and Materials Sciences Division, Lawrence Berkeley National Labs, Berkeley, California 94720-1460.

[2]Department of Chemistry and Biochemistry and the Biodesign Institute, Arizona State University, Tempe AZ 85287.

Abstract

Self-assembly has proven to be one of the most effective ways to arrange matter at the nanometer level. Biology, in particular, makes extensive use of self-assembly to position molecules over several length scales with a high degree of spatial control over structure. In recent years, one promising approach that takes advantage of biological self-assembly in order to build synthetic materials employs virus capsids, the protein shells that encapsulate the genetic material of viruses.[1] Capsids are composed of multiple protein subunits that can assemble (either spontaneously or under an external stimulus) into a monodisperse structure with different geometries depending on the virus. By appropriately functionalizing the proteins that comprise the capsid, multiple copies of a molecule or other entity can be positioned with a predictable arrangement. A wide variety of components have been attached to and arranged by virus capsids, including chromophores,[2] catalysts,[3] nanoparticles and quantum dots,[4] polymers,[5] drug molecules,[6] and imaging agents.[7]

Integrating virus capsid-based materials into higher-order structures, however, remains a challenge and a limitation to their use in many materials applications. A number of groups have investigated various techniques for patterning capsids on larger length scales, including cysteine conjugation to gold surfaces to create a monolayer of capsids,[8] DNA-based aggregation of functionalized capsids,[9] and dip-pen nanolithography[10] or nanografting[11] to introduce patterns of reactive handles on surfaces for virus immobilization. It is difficult to use these methods, however, to control the inter-capsid spacing and position individual capsids with nanoscale precision.

In order to achieve such control, we sought a scaffold that could selectively and efficiently immobilize virus capsids and order them into hierarchical structures, and we chose DNA origami[12] for this purpose. In this method, a long single-stranded piece of DNA (usually the bacteriophage M13 genome) is folded into an arbitrary two-dimensional shape using a large number of short “staple” strands. The predictable and programmable properties of DNA hybridization allow for a high degree of control and the design of virtually any geometry desired. Furthermore, it is possible to synthesize staple strands that contain an extra single-stranded “probe” sequence that extends from the origami structure. The addition of components functionalized with DNA complementary to the probes allows for their immobilization on the origami tile with a high degree of spatial control. It should also be

*denotes corresponding author hao.yan@asu.edu, francis@cchem.berkeley.edu.
‡denotes equal contribution.

possible to create higher order structures by by adding linker strands to connect the origami tiles together. As a final consideration, the size scale of DNA origami (~100 nm) is compatible with that of many virus capsids, facilitating the integration of the two components, unlike other DNA-based scaffolds that are too small to effectively order such large objects.

DNA origami has been used effectively to direct the self-assembly of nanoscale objects such as gold[13] and silver[14] nanoparticles, RNA molecules,[15] or carbon nanotubes[16] with exquisite precision. In addition, several groups have immobilized small proteins on origami tiles using a variety of approaches, including aptamer binding,[17] His_6 tags,[18] or biotin-streptavidin.[19] Our work represents the first attempt, to our knowledge, to attach a large, multi-protein entity like a virus onto an origami tile. For the capsid, we chose bacteriophage MS2, an icosahedral *E. coli* virus comprised of 180 identical protein subunits that spontaneously assemble into spherical particles 27 nm in diameter.[20] The coat protein can be expressed recombinantly, allowing for site-directed mutagenesis, and is purified as a fully assembled capsid devoid of genetic material. Access to the interior is afforded by thirty-two 2 nm holes, allowing for orthogonal functionalization of the interior and exterior surfaces by modifying the appropriate amino acid residues.[21,3a] As a result, these capsids are attractive targets as molecular containers or scaffolds for multiple copies of different components.

We recently reported a method to modify the inside of the capsid with maleimide reagents (at a mutagenically introduced cysteine) and the exterior of the capsid with single-stranded DNA using an oxidative coupling reaction that targets an unnatural amino acid introduced via amber codon suppression (Figure 1A).[21,22] By functionalizing the exterior of the capsid with DNA complementary to single-stranded probes extending from the DNA origami construct, the capsids should be able to bind the origami tile via Watson-Crick base pairing. For this work, we modified the interior of MS2 with a fluorescent dye (Oregon Green maleimide, as previously reported[3a]) to approximately 100% modification, installing 180 copies of the molecule. In these experiments, the dye serves as a model cargo; in principle, however, any maleimide reagent that can fit through the 2 nm holes can be introduced. We next modified the exterior of the capsids with a 20-nt poly-T sequence to ~11% modification, installing approximately 20 copies per capsid. The capsids remained intact, hollow, and 27 nm in diameter after both interior and exterior modification (see Supporting Information (S.I.) Figure S4 for characterization of the dual-surface modified MS2 conjugate).

For the DNA origami tile, we explored two different geometries: 1) rectangles, 90 nm in length by 60 nm in width, and 2) equilateral triangles, 120 nm on a side with a 40 nm triangular hole in the center. For the rectangles, we placed probes on either the edge (E), or middle (M) of the tile in order to demonstrate control over the exact location of the immobilized capsid on the tile. Similarly, for the triangles, we added probes to either one side (Tri1) or to all three sides (Tri3). The probes consisted of a 40-nt poly-A sequence, allowing the capsids with the 20-nt poly-T sequence to bind via complementary DNA pairing. We selected a 40-nt sequence in order to also provide a spacer between the negatively charged tile and the negatively charged capsid-DNA conjugate in order to reduce electrostatic and steric repulsion as much as possible. The multiple probe strands on each tile (3 for E tiles, 5 for Tri1 tiles, 6 for M tiles, and 15 for Tri3 tiles; see S.I. Figures S1 and S2 for tile designs and probe locations), and the multiple complementary strands on the capsids allow for multivalent binding and thus stronger association of the two components.

In order to attach the capsids to the tiles, we mixed the components in a 2:1 ratio and annealed the mixture from 37 to 4 °C at a rate of 1 °C/min to help facilitate binding. The DNA origami templated viral capsid structures were verified by atomic force microscopy

(AFM), allowing us to distinguish the tile shape from the much taller spherical capsid. To determine the efficiency of tile association with capsids a large number of AFM images were inspected to determine the fraction of tiles with capsids bound to them. After annealing, the rectangular tiles showed virtually complete association of tiles with capsids, with 97.5% of E tiles and 98.1% of M tiles bearing an MS2 capsid (Figure 2A,B). For the E tiles, the capsids were clearly attached to the edge of the tile, where the probes were located. Similarly, for the M tiles the capsids were located in the middle of the tile, demonstrating the DNA-specific association and the ability to position the capsids precisely. Analyzing the height profile of a capsid on a tile demonstrated a spherical object around 35 nm in diameter (slightly larger than the 27 nm diameter of the capsid, due to lateral broadening by the AFM tip) attached on the origami tile 1.5–2 nm in height, as expected for the width of the DNA double helix. The height of the capsids was around 12 nm, resulting from the collapse and concomitant flattening of the hollow structure on the mica surface used for AFM.

Because the capsids display approximately 20 copies of the ssDNA, multiple tiles can, in principle, bind to a single capsid. Roughly 18% of the E tiles were associated with a capsid already bound to a tile, whereas about 10% of the M tiles showed similar aggregation. This disparity between the designs is not surprising given that there is less surface area exposed and thus less electrostatic repulsion when two tiles approach one another from the side, as is the case with the E tiles, compared to face-on, as with the M tiles.

Using only one equivalent of MS2 (relative to the tile) resulted in around 89% of E tiles and only 70% of M tiles bearing a capsid. The higher efficiency of association for E tiles is again consistent with a lower amount of charge repulsion involved in an edge-on approach of the tile to the capsid. Because the origami tiles serve as the structural element to arrange the capsids, we wanted complete modification of the tiles with capsids, so we used two equivalents of MS2 for all further experiments. Current studies are under way to determine a method to purify MS2 not associated with a tile from the desired tile-capsid conjugates.

Control experiments with capsids without DNA showed no association with the tiles, indicating that the association was not due to some other non-specific effect (S.I. Figures S15–S17). Similarly, mixing tiles bearing DNA that did not complement the sequences on the capsids also showed no significant association of the two components (S.I. Figure S18). Furthermore, binding capsids to the tiles and then adding excess 40-nt polyT ssDNA (which should bind to the 40-nt polyA probe with greater affinity than the 20-nt sequence on the MS2) removed the capsids from the tile (S.I. Figure S19). This experiment not only confirmed the specific DNA-based association, but also indicates a potential mechanism for releasing the capsids from the tiles if desired.

The triangular tiles proved equally efficient at binding capsids as the rectangular tiles. Exposing the Tri1 tiles to two equivalents of MS2 and annealing as above resulted in virtually 100% association of capsids to the tiles (Figure 2C). The capsids are bound to a single side of the triangular tile and the hole in the center is clearly visible by AFM. The triangular shape of the tiles allowed facile visualization by transmission electron microscopy (TEM) as well and the electron micrographs further confirm the association of the capsids to a single side of the triangular tile. The Tri3 tiles showed a similarly high hybridization efficiency (~100%), but in this design anywhere between one and three capsids can bind to each tile. The majority of samples visualized by AFM and TEM, however, showed a single capsid bound in the central hole of the tile (Figure 2D). We believe that once the capsid binds to one side of the triangular tile, the extra DNA strands on its surface quickly hybridize to the probes on the other two sides due to the increased local concentration effect. This hypothesis is supported by the fact that the sides of the Tri3 tiles appear to be contracted towards the center, suggesting that the capsid (which is smaller than the 40 nm

hole in which it sits) pulls the sides inwards by binding to all three. Some Tri3 tiles were observed bearing one capsid on a single side (instead of in the hole), one capsid on each of two sides, or one capsid on each of three sides (see S.I. Figure S9), but the majority of the tiles visualized showed a single capsid in the center.

It is important to note that the polyA/T strategy used was necessary for obtaining the high efficiency of capsid association in these results. Similar experiments using a randomly chosen complementary DNA sequence resulted in only around 50% association of capsids with E tiles (see S.I. Figure S27), and increasing the amount of MS2 added or the annealing time did not result in increased efficiency. We believe that the polyA/T strategy is particularly effective because the strands on the MS2 can bind only one or two bases of the probe initially and then "slide" along the probe to find the thermodynamically optimum conformation.[23] Furthermore, different strands on the capsid can bind the probe strand with less than 20 base pairs, promoting multivalent binding without requiring complete hybridization. Although it would seem that the polyA/T strategy will only allow for one type of capsid to be immobilized, we believe that any short repeating sequence would allow for a similar "sliding" mechanism and thus efficient binding. This would allow multiple types of capsids, bearing different groups on the interior, for example, to be patterned.

Having successfully immobilized capsids on origami tiles with high efficiency, we next sought to use the DNA scaffold to organize the capsids on a larger length scale. As a proof of principle, we decided to create a one-dimensional array of capsids by linking the supporting origami tiles together. We designed two sets of strands, each of which partly binds to the M13 genome on opposite corners of the rectangular origami tile. These two sets contain complementary sequences, linking tiles at their corners and arranging them in a step-like array. We hypothesized that we could use this method with the E and M tiles to create a one-dimensional array of capsids with defined nanoscale separation.

Mixing the tiles (E or M), capsids, and linkers together and annealing from 37 to 4 °C at a rate of 1 °C/min resulted in the expected arrays of tiles while retaining the virtually 100% association efficiency of the capsids (Figure 3A,B). The AFM images clearly show a one-dimensional arrangement of capsids either on the edge or in the middle of the tiles (for E and M tiles, respectively) separated by approximately 100 nm. About 50% of the tiles formed arrays of at least two tiles, and the percentage of tiles in a given array decresed with increasing length (see S.I. Figures S20 and S21 for length distributions). However, we occasionally observed arrays of five or six tiles, all the while maintaining the spacing between the capsids. Doubling the linker concentration resulted in a higher proportion of tiles in arrays (~60%). It was also possible to create the arrays in a hierarchical, rather than one-pot, procedure by annealing the capsids to the tiles first and then adding the linkers to form arrays in a second annealing step. Once again, arrays formed readily, though slightly fewer tiles (~45%) were in arrays greater than two. This decrease is likely due to the increased steric or electrostatic demands of linking tiles with capsids already bound (see S.I. Figures S20 and S21 for summaries of the percentage of tiles in arrays two tiles or greater).

Because the E tiles experience less repulsion when two tiles bind a single capsid compared to the M tiles (Figure 1A,B), we saw numerous instances of two E tile arrays that were linked by one set of capsids (see Figure 3A, top zoom-in). Also, once a single tile in an E-tile array binds a capsid on another array, the other tiles are perfectly positioned to bind adjacent capsids. The M tile arrays, by comparison, do not suffer as much from these drawbacks and result in structures with markedly less inter-array aggregation.

We also formed arrays of E and M tiles without any MS2 in order to compare the efficiency of the process with and without the capsids present. We found that in both cases, a higher

proportion of tiles were incorporated into arrays (65–68% compared to ~50% for arrays with MS2), and that the arrays tended to be longer, with a few instances of eight or nine tiles in a row (see S.I. Figures S13 and S14 for AFM images of arrays without MS2, and Figures S20 and S21 for length distributions). We attribute this improvement to the decreased steric and electrostatic repulsion between tiles when capsids were not present.

In light of these results, we sought to first form longer arrays with tiles alone, and then in a second step add capsids to bind to the probes on the arrays. With the E tiles, this strategy resulted in a great degree of inter-array aggregation, as multiple arrays were connected by a single set of capsids. As a result, very few single arrays were observed, and a majority of arrays clumped together into amorphous aggregates (data not shown).

The M tiles, by contrast, proved much more effective for this strategy due to their lower propensity to form aggregates. Long arrays of capsids, occasionally reaching nine or ten capsids in length, were observed, Figure 3C. Furthermore, because the linkers were still present in solution during the second annealing step (to attach the capsids to the arrays), the arrays were able to grow yet longer and incorporate even more tiles into arrays of two tiles or longer (~75%: for length distribution, see S.I. Figure S21). Unlike the one-pot annealing results, however, doubling the concentration of linkers did not result in increased array lengths or an increased percentage of tiles in arrays.

The hierarchical self-assembly in forming the E and M tile arrays is a competition between productive assembly (the capsids associating with the tiles and the tiles forming arrays) and unproductive assembly (multiple tiles binding to a single capsid, resulting in aggregation). Annealing for a longer time (1 °C/2 min) resulted in a much higher degree of aggregation, and significantly fewer well-formed arrays. Furthermore, although it was possible to create remarkably long arrays by annealing the tiles only (without MS2) for much greater lengths of time (45 to 4 °C at a rate of 1 °C/10 min), the resulting arrays were too flexible, and upon addition of MS2 different sections of the arrays folded back on themselves and bound to a single capsid, again resulting in undesired and intractable aggregates.

The E tiles demonstrated the facility of binding multiple tiles to a single capsid when the probes are located at the edge of the tile. Although this was a liability in the linker-based array formation, we decided to capitalize on this property by designing another rectangular tile with a set of five 40-nt polyA probes on both short ends (see S.I. Figure S1). We envisioned that this design would allow for two tiles to be linked by a single capsid, creating a “daisy-chain” (DC) array of alternating capsids and tiles. In order to promote association of the tiles further via noncovalent base stacking interactions, we added the staple strands for the short edges of the tiles into the annealing mixture. We hypothesized that this stacking would pre-organize the tiles into short linear arrays, further facilitating the capsids in linking them.

Annealing a mixture of DC tiles, capsids (again, two equivalents), and edge staples from 37 to 4 °C at a rate of 1 °C/min resulted in the expected formation of arrays of tiles linked by capsids, with approximately 90–100 nm spacing between capsids (Figure 3D). The efficiency was remarkably high, with only a small fraction of tile edges (~6%) that were not associated with a capsid. The length distribution of arrays peaked at three capsids in a row (separated by two tiles), and decreased thereafter (see S.I. Figure S22 for length distribution), but some arrays of ten or more capsids were observed. Occasionally, three or four tiles bound to a single capsid resulting in branching arrays; however, only a small fraction of capsids (~5%) served as such branching points, and the vast majority bound only two tiles. The arrays usually formed in a linear fashion (most likely to minimize repulsion between tiles), but because the tiles could bind to any location on the capsid, occasionally

the tiles bound the capsids with an angle less than 180°, resulting in kinks in the arrays. Omitting the edge staples resulted in shorter arrays (data not shown), indicating the usefulness of these staples in promoting array formation.

We note that the DC tile design represents a complementary approach to forming capsid arrays compared to the linker-based approach for the E and M tiles. In the latter case, an external stimulus (i.e. the addition of the linker strands) induces assembly into higher-order structures, whereas in the former case the actual capsid binding event is the stimulus for array growth through a condensation polymerization-like mechanism. Depending on the application at hand, one strategy or the other may prove more useful. (For additional AFM images of all experiments shown in Figures 3A–D, see S.I. Figures S10–S12).

In order to further characterize the conjugates, we obtained TEM images of both the M and DC tile arrays (see S.I. Figures S25 and S26). Although the rectangular tiles are not easily visualized in TEM, we were able to obtain images that clearly showed the hollow capsids spaced approximately 100 nm apart. The arrays most often adsorbed to the TEM grid edge-on, so the tiles appeared as dark lines connecting the capsids. The tiles were often twisted when deposited on the TEM grid, but these results further confirm that the capsids remained intact during the array formation.

One of the great advantages of our approach lies in its versatility due to the modular nature of the capsid modification and the high degree of programmability intrinsic to DNA-based nanostructures. By choosing the appropriately designed tile, virtually any geometry is possible, and the capsids can be placed in any location on that tile. Furthermore, the interior of the capsid can be modified with a wide variety of reagents, allowing for introduction of imaging agents, catalysts, or nucleation sites for nanoparticle growth. The one-dimensional arrays made possible by the origami tiles thus create the possibility of patterning arrays of nanoscale reactors, drug carriers (with programmed release by strand displacement), or metal particles for plasmonic arrays, all with high precision.

Finally, we stress the size and complexity of the components involved in these experiments. The MS2 capsids are 2.5 MDa, spherical objects 27 nm in size, self-assembled from 180 protein monomers, covered in ssDNA and containing chromophores inside on each monomer at specified locations. The DNA origami tiles are 4.8 MDa objects with dimension around 100 nm, comprised of hundreds of individual DNA strands self-assembled into a well-defined geometry. Yet these two components come together in a predictable manner, with high efficiency and specificity, under mild conditions in only 30 minutes. Furthermore, the conjugates can then be used to build higher order structures approaching a micron in length (for arrays of ten tiles, for example). We believe that the programmability of origami scaffolds and the ability to modify large protein constructs with single-stranded DNA will allow for the construction of increasingly complex and integrated biomolecular systems in the future, and pave the way for a variety of interesting nanotechnology applications.

Supplementary Material

Refer to Web version on PubMed Central for supplementary material.

Acknowledgments

Research efforts for N.S. and M.B.F. were supported by the Director, Office of Science, Materials Sciences and Engineering Division, of the U.S. Department of Energy under Contract No. DE-AC02-05CH11231. H.Y. acknowledges funding from the NIH, ONR, ARO, NSF, DOE and the Sloan Research Foundation. H. Y. and Y.L. were supported as part of the Center for Bio-Inspired Solar Fuel Production, an Energy Frontier Research Center funded by the U.S. Department of Energy, Office of Science, Office of Basic Energy Science under Award Number DE-SC0001016. M.L., Z.L., Y.L., and H.Y. would like to thank Suchetan Pal and Zhao Zhao for assistance with

TEM and the EM facility in the School of Life Sciences at Arizona State University, and Yonggang Ke for helpful discussions. N.S., G.J.T., and M.B.F. would like to thank David Unruh and Prof. Jean Fréchet for assistance with and use of their AFM.

References

1. a) Douglas T, Young M. Science. 2006; 312:873–875. [PubMed: 16690856] b) Fischlechner M, Donath E. Angew. Chem. Int. Ed. 2007; 46:3184–3193.
2. a) Wang Q, Lin T, Tang L, Johnson JE, Finn MG. Angew. Chem. Int. Ed. 2002; 41:459–462.b) Demir M, Stowell MHB. Nanotechnology. 2002; 13:541–544.c) Schlick TL, Ding ZB, Kovacs EW, Francis MB. J. Am. Chem. Soc. 2005; 127:3718–3723. [PubMed: 15771505] d) Miller RA, Presley AD, Francis MB. J. Am. Chem. Soc. 2007; 121:3104–3109. [PubMed: 17319656] e) Endo M, Wang H, Fujitsuka M, Majima T. Chem. Eur. J. 2006; 12:3735–3740.f) Miller RA, Stephanopoulos N, McFarland JM, Rosko AS, Geissler PL, Francis MB. J. Am. Chem. Soc. 2010; 132:6068–6074. [PubMed: 20392093]
3. a) Stephanopoulos N, Carrico ZM, Francis MB. Angew. Chem. Int. Ed. 2009; 48:9498–9502.b) Nam YS, Magyar AP, Lee D, Kim J-W, Yun DS, Park H, Pollom TS Jr. Weitz DA, Belcher AM. Nature Nanotech. 2010 published online 4/11/10.
4. a) Douglas T, Young MJ. Nature. 1998; 393:152–155.b) Douglas T, Strable E, Willits D, Aitouchen A, Libera M, Young M. Adv. Mater. 2002; 14:415–418.c) Loo L, Guenther RH, Basnayake VR, Lommel SA, Franzen S. J. Am. Chem. Soc. 2006; 128:4502–4503. [PubMed: 16594649] d) Loo L, Guenther RH, Lommel SA, Franzen S. J. Am. Chem. Soc. 2007; 129:11111–11117. [PubMed: 17705477] e) Dixit SK, Goicochea NL, Daniel M-C, Murali A, Bronstein L, De M, Stein B, Rotello VM, Kao CC, Dragnea B. Nano Lett. 2006; 6:1993–1999. [PubMed: 16968014]
5. a) Kovacs EW, Hooker JM, Romanini DW, Holder PG, Berry KE, Francis MB. Bioconjugate Chem. 2007; 18:1140–1147.b) Comellas-Aragonès M, Escosura A, Dirks AJ, van der Ham A, Fusté-Cuñé A, Cornelissen JJLM, Nolte RJM. Biomacromolecules. 2009; 10:3141–3147. [PubMed: 19839603] c) Abedin MJ, Liepold L, Suci P, Young M, Douglas T. J. Am Chem. Soc. 2009; 131:4346–4354. [PubMed: 19317506]
6. a) Wu W, Hsiao SC, Carrico ZM, Francis MB. Angew. Chem. Int. Ed. 2009; 48:9493–9497.b) Manchester M, Singh P. Adv. Drug Deliver. Rev. 2006; 58:1505–1522.c) Suci PA, Varpness Z, Gillitzer E, Douglas T, Young M. Langmuir. 2007; 23:12280–12286. [PubMed: 17949022] d) Flenniken M, Uchida M, Liepold L, Kang S, Young M, Douglas T. Viruses Nanotechnol. 2009; 327:71.
7. a) Anderson EA, Isaacman S, Peabody DS, Wang EY, Canary JW, Kirshenbaum K. Nano Lett. 2006; 6:1160–1164. [PubMed: 16771573] b) Hooker JM, Datta A, Botta M, Raymond KN, Francis MB. Nano Lett. 2007; 7:2207–2210. [PubMed: 17630809] c) Hooker JM, O'Neil JP, Romanini DW, Taylor SE, Francis MB. Mol. Imaging Biol. 2008; 10:182–191. [PubMed: 18437498]
8. Klem MT, Willits D, Young M, Douglas T. J. Am. Chem. Soc. 2003; 125:10806–10807. [PubMed: 12952458]
9. Strable E, Johnson JE, Finn MG. Nano Lett. 2004; 4:1385–1389.
10. Smith JC, Lee K-B, Wang Q, Finn MG, Johnson JE, Mrksich M, Mirkin CA. Nano Lett. 2003; 3:883–886.
11. Cheung CL, Camarero JA, Woods BW, Lin T, Johnson JE, De Yoreo JJ. J. Am. Chem. Soc. 2003; 125:6848–6849. [PubMed: 12783520]
12. Rothemund PWK. Nature. 2006; 440:297–302. [PubMed: 16541064]
13. a) Ding B, Deng Z, Yan H, Cabrini S, Zuckermann RN, Bokor J. J. Am. Chem. Soc. 2010; 132:3248–3249. [PubMed: 20163139] b) Sharma J, Chhabra R, Andersen CS, Gothelf KV, Yan H, Liu Y. J. Am. Chem. Soc. 2008; 130:7820–7821. [PubMed: 18510317]
14. Pal S, Deng Z, Ding B, Yan H, Liu Y. Angew. Chem. Int. Ed. 2010; 122:2760–2764.
15. Ke Y, Lindsay S, Chang Y, Liu Y, Yan H. Science. 2008; 319:180–183. [PubMed: 18187649]
16. Maune HT, Han S, Barish RD, Bockrath M, Goddard WA III, Rothemun PWK, Winfree E. Nat. Nanotech. 2010; 5:61–66.

17. a) Rinker S, Ke Y, Liu Y, Chhabra R, Yan H. Nat. Nanotech. 2008; 3:418–422.b) Chabra R, Sharma J, Ke Y, Liu Y, Rinker S, Lindsay S, Yan H. J. Am. Chem. Soc. 2007; 129:10304–10305. [PubMed: 17676841]
18. Shen W, Zhong H, Neff D, Norton ML. J. Am. Chem. Soc. 2009; 131:6660–6661. [PubMed: 19400586]
19. Kuzuya A, Kimura M, Numajiri K, Koshi N, Ohnishi T, Okada F, Komiyama K. ChemBioChem. 2009; 10:1811–1815. [PubMed: 19562789]
20. a) Hooker JM, Kovacs EW, Francis MB. J. Am. Chem. Soc. 2004; 126:3718–3719. [PubMed: 15038717] b) Valegård K, Liljas L, Fridborg K, Unge T. Nature. 1990; 345:36–41. [PubMed: 2330049] c) Mastico RA, Talbot SJ, Stockley PG. J. Gen Virol. 1993; 74:541–548. [PubMed: 7682249]
21. Tong GJ, Hsiao SC, Carrico ZM, Francis MB. J. Am. Chem. Soc. 2009; 131:11174–11178. [PubMed: 19603808]
22. Mehl RA, Anderson JC, Santoro SW, Wang L, Martin AB, King DS, Horn DM, Schultz PG. J. Am. Chem. Soc. 2003; 125:935–939. [PubMed: 12537491]
23. Le JD, Pinto Y, Seeman NC, Musier-Forsyth K, Taton TA, Kiehl RA. Nano Lett. 2004; 4:2343–2347.

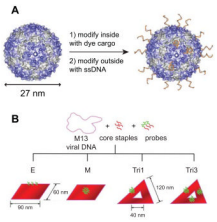

FIGURE 1.

Summary of the components integrated in this work. (A) Bacteriophage MS2 capsids were modified on the interior with fluorescent dyes and on the exterior surface with ssDNA. (B) Several different DNA origami tiles were constructed with different geometries and probe locations. The ssDNA probes were complementary to the DNA strands on the capsids, directing the association of the two components.

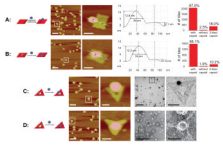

FIGURE 2.

Association of origami tiles with MS2 capsids using DNA-based hybridization. (A) E tiles + MS2, L-R: zoom-out AFM image, zoom-in AFM image, height profile of zoom-in image, and characterization of association efficiency. (B) M tiles + MS2, L-R: zoom-out AFM image, zoom-in AFM image, height profile of zoom-in image, and characterization of association efficiency. (C) Tri1 tiles + MS2, L-R: zoom-out AFM image, zoom-in AFM image, zoom-out TEM image, zoom-in TEM image. (D) Tri3 tiles + MS2, L-R: zoom-out AFM image, zoom-in AFM image, zoom-out TEM image, zoom-in TEM image. Zoom-out scale bars: 200 nm. Zoom-in scale bars: 50 nm.

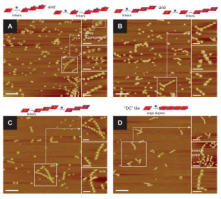

FIGURE 3.

AFM images of MS2 arrays formed by origami tiles. (A) E tiles + MS2 + linkers (one-pot annealing) and E tiles + MS2, followed by the addition of linkers in a second step. (B) M tiles + MS2 + linkers (one-pot annealing) and M tiles + MS2, then addition of linkers in a second step. (C) M tiles + linkers, then addition of MS2 in a second step. (D) DC tiles + MS2 + edge staples (to encourage tile edge stacking). The top image of the three zoom-ins corresponds to the indicated area of the zoom-out; the other two zoom-in images come from different areas (see Supporting Info for additional zoom-out images). Zoom-out scale bars: 500 nm. Zoom-in scale bars: 200 nm.